euspen's 24th International Conference & Exhibition, Dublin, IE, June 2024
www.euspen.eu

Evaluation of the measurement uncertainty of a high-precision telescopic instrument for machine tool verification

Francisco Javier Brosed[1,2,3], Juan José Aguilar[1,2], Raquel Acero[1,2], Sergio Aguado[1,2], Marcos Pueo[1,2]

[1]*Department of Design and Manufacturing Engineering, University of Zaragoza, María de Luna 3, 50018 Zaragoza, Spain.*
[2]*Instituto de Investigación en Ingeniería de Aragón (I3A), 50018 Zaragoza, Spain*
[3]*fjbrosed@unizar.es*

Abstract

Precision measuring instruments and the ability to track measurement results to verify production systems in accordance with national and international standards are key tasks in the manufacturing industry. There are instruments on the market that allow the measurement of three-dimensional coordinates using telescopic systems. Typically, from three multi-cycle measurements of the head position, using a single telescopic system, or from a single measurement, using three telescopic systems during a simultaneous measurement process. These are products used to verify the behaviour of machine tools and robots. The work presented in this paper shows the modelling of the measurement system to evaluate its uncertainty and the effect on it of different system configuration options. The measurement system is based on a multilateration process that starts by measuring distances with several telescopic systems simultaneously. The evaluation of the influence of the configuration on the measurement uncertainty will include the distances between the reference points for multilateration and the angles formed by the telescopic systems.

Measurement uncertainty, machine tool multilateration, Interferometric multilateration, Monte Carlo simulation.

1. Introduction

Precision measurements in manufacturing systems are a key factor for advanced technologies [1]. In the optimization process of the manufacturing systems, the verification techniques allow the measurement and compensation of machine tool (MT) errors [2]. Furthermore, the high precision dimensional metrology [3,4] has become essential for the manufacturing industry [5] due to tighter geometric tolerances in the manufactured products. In this frame, the traceability of the measurement results is needed to improve the behaviour of the manufacturing systems and guarantee the quality in the production process [6].

MT verification can be carried out measuring the MT head position with measuring instruments such as interferometers [7], measuring distances following the axis directions of the MT; ball bars [8], measuring circular trajectories of the MT; laser tracers [9] and laser ball bars [10, 11] that measure the distance from a fixed point in the MT table to the MT head running several cycles, varying the position of the fixed point to the MT table, to measure the position of the MT head; and laser trackers [12] using the distance measured to a retroreflector and the angles from its angular encoders to measure the position of the MT head.

The measurement system to be analysed in this paper can be classified in the laser ball bar group, but with the special feature of allowing the measurement of the MT position in a single cycle. The measurement system (Telescopic Simultaneous Ballbar, TSB) uses three telescopic arms to simultaneously measure the distance from three spheres in the MT table to one sphere in the MT head, achieving verification process times similar to those obtained with the use of a laser tracker, but improving the precision of the measurement result compared to the precision obtained with non-simultaneous laser ball bars because the positioning repeatability of MT will not affect the triangulation calculation as occurs with laser tracers [9].

A calibration and uncertainty budget analysis for the TSB is presented in [13] but an analysis of the variation of the measurement uncertainty in the verification field depending on the spatial distribution of the three spheres fixed to the MT table is needed to assure the traceability of the measurement results obtained with the TSB using different spatial configurations in the MT table.

The main goal of this work is to evaluate the correlation between the measurement uncertainty value of the TSB and the position of the target points (TGs) in the verification volume. To achieve this objective, the behaviour of the TSB has been simulated and its measurement uncertainty has been estimated, with the Monte Carlo method [14,15], for different spatial distributions of the three spheres in the MT table.

The paper is structured as follows: Section 2 describes the TSB and the mathematical model used to estimate its uncertainty. Section 3 details the methodology followed in the analysis and the settings of each test simulated. Section 4 present the uncertainty obtained for each scene simulated. Finally, Section 5 shows the main conclusions of the study.

2. *Measurement system* description

The TSB is a measurement system composed by three telescopic arms. Each telescopic arm measure the distance between two spheres using a laser interferometer integrated in the telescopic arm (measurement uncertainty of the laser interferometer, Attocube IDS3010, with a coverage factor of two is 0.3 µm using an environmental compensating unit). For the measurement of a point in the space (i.e.: the centre of a sphere in the MT head) one end of each of the three telescopic arms is placed on a surface (i.e.: the MT table), so that their relative distances remain constant. This end of each of the telescopic arms is a sphere joined with the surface where is placed through

a kinematic support that allows the rotation of the arm keeping the sphere centre static. The other end of the telescopic arms is a multi-point kinematic coupling especially developed for the TSB [16] that allows the connection of the three telescopic arms with a single sphere simultaneously. This configuration of the TSB enable the calculation of the single sphere centre position using multilateration.

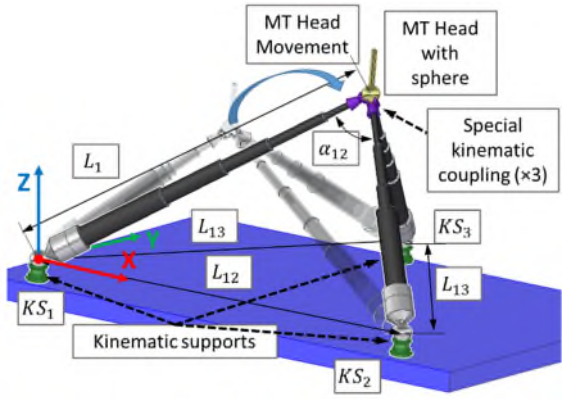

Figure 1. Example of the configuration of the TSB in the position measurement process using multilateration and main parameters of the model. The parameters L_2, L_3, α_{13} and α_{23} have been omitted in the figure to improve the visibility, but can be easily deduced.

The main error sources considered to simulate the behaviour of the TSB are: the geometric error of the TSB spheres, the measurement bias of the telescopic arms with the inclination and the rotation angles, the errors in the compensation of the temperature and the uncertainty of the telescopic arms measuring distances between centres. The measurement uncertainty obtained from this error sources following the methodology explained in [13] for a TSB's telescopic arm measuring distances in workshop conditions is 4 µm (with a confidence level of two, k=2) and the measurement range for each arm goes from 411 mm to 1040 mm. From this input data the simulation tests, explained in the following section, have been carried out.

3. Methodology and simulation test

The measurement of the position of a sphere (generally linked to the MT head) with the TSB requires previously measuring of the distance between each of the three kinematic supports (KS_i, with i from 1 to 3). The three distances, L_{ij}, with i and j from 1 to 3 and $i \neq j$, are the distances with which the reference system is build. This reference system is the one used to express the three dimensional coordinates of the centre of the sphere that are obtained as result of the measurement with the TSB. From L_{ij} the coordinates of each kinematic support, KS_i, can be calculated, equations (1), (2) and (3).

$$X_{KS2} = L_{12} \quad (1)$$
$$X_{KS3} = L_{13} \cdot \cos(\beta_{13}) \quad (2)$$
$$Y_{KS3} = L_{13} \cdot \sin(\beta_{13}) \quad (3)$$

Where β_{13} is the angle between the segment joining KS_1 and KS_2 with the segment joining KS_1 and KS_3. The values of the rest of coordinates of KS_i are zero: The centre of the sphere in KS_1 is defined as the origin of the reference system, KS_2 defines, together with the origin, the X axis and the three KS_i define the XY plane of the reference system.

The coordinates of the centre of the sphere in the MT header are obtained via multilateration as the intersection of three spheres, equations (4), (5) and (6).

$$X = \frac{{L_1}^2 - {L_2}^2 + {X_{KS2}}^2}{2 \cdot X_{KS2}} \quad (4)$$
$$Y = \frac{{L_1}^2 - {L_3}^2 + {X_{KS3}}^2 + {Y_{KS3}}^2}{2 \cdot Y_{KS2}} - \frac{X_{KS3}}{Y_{KS3}} \cdot X \quad (5)$$
$$Z = \sqrt{{L_1}^2 - X^2 - Y^2} \quad (6)$$

Where L_i, with i from 1 to 3, are the distances between spheres measured by the telescopic arm i of the TSB.

From equations (1) to (6) could be seen that the calculation process for obtaining the position of the sphere in the MT Head depends on the length measurement of each telescopic arm of the TSB (L_i and L_{ij}). Therefore, the effect of the measurement uncertainty of the telescopic arms of the TSB is simulated and the uncertainty of the measurement of the position of the sphere in the MT head is estimated using the Monte Carlo Method [15].

A configuration of the supports forming an equilateral triangle has been assumed and the measurement uncertainty has been estimated for different sizes of the triangle. The side of the triangle has been varied from 500 mm in 100 mm increments to a maximum of 1000 mm. A total of six cases, designed with the letters from A to F have been studied, table 1.

Table 1. Sizes of the equilateral triangle formed by the kinematic supports, KS_i. A total of six cases are studied. The values under each letter indicates the size of the triangle side, L_{ij}, and the number of target points, TG.

Case	A	B	C	D	E	F
L_{ij}/mm	500	600	700	800	900	1000
TG	181	208	214	214	214	213

The target points (TGs) in the TSB verification volume have been obtained by varying the lengths of the arms from 500 mm in 100 mm increments to a maximum of 1000 mm so that a representative verification volume of the TSB was covered, figure 2.

The measurement uncertainty of the TSB has been evaluated for the TGs within the verification volume in the six cases (from A to F) recording, in addition to the uncertainty obtained in the X, Y, Z directions of the reference system (U_X, U_Y, U_Z), the position of the TGs and the angles that the arms formed with each other (α_{ij}, with i and j from 1 to 3 and $i \neq j$).

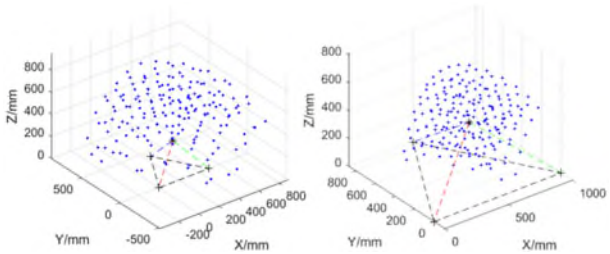

Figure 2. TSB Verification Volume for different sizes (500mm and 1000 mm) of the triangle formed by the kinematic supports (black cross and black dashed line).

The number of iterations is an important parameter of the Monte Carlo simulation. If the number of iterations is low the results obtained diverge when the test is repeated. If the number of iterations is high enough the results converge to the same solution but if the number of iterations is excessively high, the time required to perform the simulation increases, which can result in unfeasible test. From previous works, the Monte Carlo simulation converge using 10^6 iterations [13].

The main results obtained from the simulation tests are the correlation of U_X, U_Y and U_Z with some of the main

configuration and characteristics of the TSB, such as: the distribution of KS_i, the coordinates of the TGs in the verification volume (blue dots in figure 2) and α_{ij}. The variation of the verification volume when L_{ij} changes can also be analysed.

4. Simulation Results

Following the methodology exposed in the previous section the simulation tests have been performed. Running 10^6 iterations for each of the six cases, 120 s for each case were enough to end the simulation with a 2.3 GHz CPU clock speed.

The measurement uncertainty within the verification volume has been estimated using Monte Carlo Method and U_X, U_Y and U_Z for each TG has been obtained.

The uncertainty variation within the verification volume can be observed in figure 3, where the results for the case A with $L_{ij} = 500\ mm$ and case F with $L_{ij} = 1000\ mm$ are shown. These are the cases with the higher values of uncertainty ($L_{ij} = 500\ mm$) and with the lower values ($L_{ij} = 1000\ mm$) of the six cases analysed. In figure 3, the colour of the target point indicates the maximum value of the uncertainty in each TG ($\max\{U_X, U_Y, U_Z\}$).

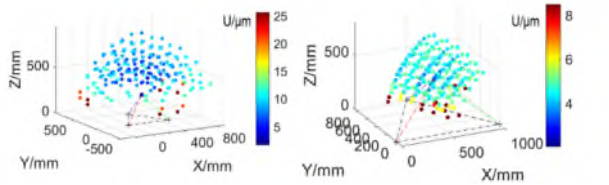

Figure 3. Measurement Uncertainty of the TSB in the verification volume. The maximum value of the uncertainty for each TG ($\max\{U_x, U_y, U_z\}$) is represented for case A, $L_{ij} = 500\ mm$, and case F, $L_{ij} = 1000\ mm$.

Despite the difference in scale presented by case A and case F showed in figure 3, that will be further explained with the next figures, similarities can be established between them, which are also applicable to the rest of the cases (from case A to case F). The maximum values of the colormap are reached only by points located in the periphery and in the lower levels of the admissible Z-axis direction. The rest of the TGs within the volume (more than 90% for all the cases) present uncertainty values for any direction, under 10 μm (k=2), for case A, and 6 μm (k=2), for case F. The other four cases (from case B to case E) are between these two values. This point can be corroborated for Cases A and F with figure 4, where the distribution of the uncertainty values are plotted for U_X, U_Y and U_Z.

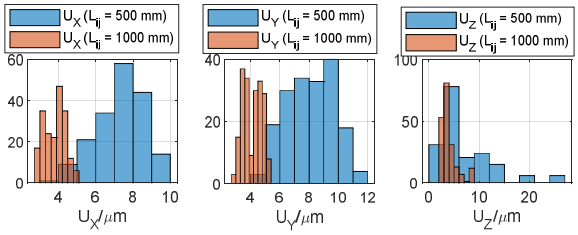

Figure 4. TSB Measurement Uncertainty distribution in X, Y and Z directions for case A ($L_{ij} = 500\ mm$) and case F ($L_{ij} = 1000\ mm$).

The distributions presented in figure 4 have been obtained with the simulation results of 181 TGs in case A and of 213 TGs in case F. First, it is confirmed what appears in figure 3, the measurement uncertainty values of the TSB are higher in case A than in case B. In addition, figure 4 allows to identify the differences between U_X, U_Y and U_Z and evaluate their distributions corroborating what was previously asserted, that more than 90% of the TGs present measurement uncertainty values for any direction, under 10 μm (k=2), for case A, and 6 μm (k=2), for case F.

By introducing cases B to E into the comparison, it is possible to observe the decrease in uncertainty values as L_{ij} increases, figure 5.

Figure 5, plots the correlation of the measurement uncertainty value (U_X, U_Y, U_Z) with the position of the TG evaluated for the six cases analysed (from case A to F), figure 5(a), and with α_{ij}, from case A to F too, figure 5(b). The first column of graphs in figure 5(a) plots the X-axis coordinate of the TG versus U_X (first row), versus U_Y (second row) and versus U_Z (third row). In the same way, in figure 5(b), the columns of the figure contains the graphs plotting α_{ij} of the TG versus U_X, first row, U_Y, second row and U_Z, third row.

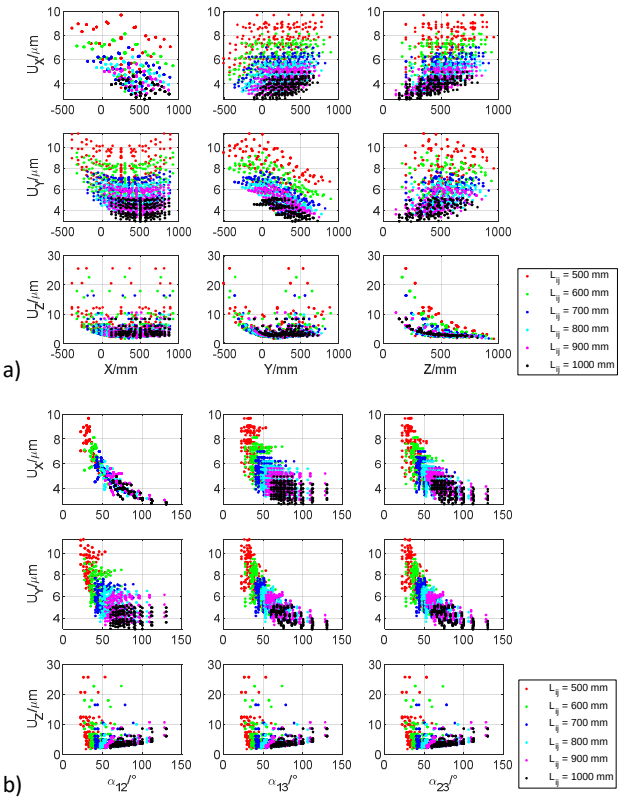

Figure 5. Measurement uncertainty value for the six cases analysed (from case A to F). (a) The coordinates of each TG (X, Y, Z) versus U_X, U_Y, U_Z. X, Y, Z coordinates are plotted in the abscissa of the graphs in the first, second and third column respectively. U_X, U_Y, U_Z uncertainties are plotted in the ordinate of the graphs of the first, second and third row respectively. (b) α_{12}, α_{13}, α_{23} for each TG versus U_X, U_Y, U_Z. α_{12}, α_{13}, α_{23} angles are plotted in the abscissa of the graphs in the first, second and third column respectively. U_X, U_Y, U_Z uncertainties are plotted in the ordinate of the graphs of the first, second and third row respectively.

There are two correlations that appear clearly: U_Z with Z-axis direction in figure 5(a) and U_X with α_{12} in figure 5(b). Although inflection points can be detected in some of the other graphs. From figure 5(a): U_X increases with X and reach a maximum with $X = L_{ij}/2$, decreasing for higher values of X and Increases with Y until reaching a stable value for $Y \geq 0$. U_Y decreases with the increase of X and reach a minimum with $X = L_{ij}/2$, increasing for higher values of X and presents a change in behaviour approximately in $Y = 0$.

In figure 5(b), the correlation between U_X and α_{12} appears clearly because, due to the reference system definition, X-axis coordinate is calculated from L_1 and L_2 and without L_3, equation (4). The correlation shows that U_X decreases when α_{12} increases.

The correlation of U_Z with the Z-axis coordinate is shown in figure 5(a) and indicates that the higher the Z value the lower the uncertainty value. This correlation appears, in a more diffuse way, in the opposite direction between U_X and U_Y and the Z-axis coordinate. This behaviour is related to the angles α_{ij}: for high Z values the angles are smaller allowing, when noise appears in the measurement results, a very precise identification of Z-axis coordinate but a less precise identification for X and Y-axis coordinates. In figure 6, the uncertainty for TGs of case F is plotted with Z-axis coordinate to clearly show this correlation that appears similar in the other cases.

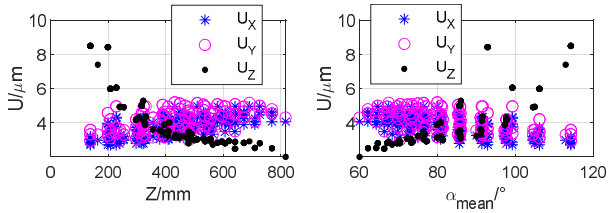

Figure 6. Measurement uncertainty value for case F ($L_{ij} = 1000\ mm$). U_X, U_Y, U_Z versus Z-axis coordinate and U_X, U_Y, U_Z versus the mean value of α_{ij} (α_{mean})

The correlation between U_Z and the angles (α_{ij}) depends on the three angles at the same time. For this reason in figure 6 the uncertainty for TGs of case F is plotted with the mean value of α_{ij} (α_{mean}). The lower values of U_Z are related to low values of α_{mean}, this happens when the target points are located in high Z-axis coordinates ($U_X \leq 4\ \mu m$ if $\alpha_{mean} \leq 80°$ or $Z \geq 500\ mm$).

5. Conclusions

The measurement results of the TSB have been simulated and its measurement uncertainty estimated to evaluate the correlation between the measurement uncertainty value of the TSB and the position of the target point in the verification volume. The measurement system (TSB) and the methodology for the simulation have been presented. The measurement uncertainty of the TSB has been estimated with Monte Carlo simulation using from 181 to 214 TGs depending on the case (six different cases, from A with $L_{ij} = 500\ mm$ to F with $L_{ij} = 1000\ mm$). The simulation with the six cases indicates that the measurement uncertainty decreases when L_{ij} increases. Although, the correlation of U_X, U_Y and U_Z with the position of the TGs and α_{ij}, has been evaluated showing these main results: Several configurations of the KS_i can be found ($L_{ij} \geq 800\ mm$) where the TSB can measure target points with a measurement uncertainty lower than 6 µm ($k = 2$) excluding the target points located in the surroundings of the physical limits of the telescopic arms (10% of the target points). The dependence of $U_X$and U_Y with X and Y-axis coordinates show inflection points with $X = L_{ij}/2$ and $Y = 0$. The correlation of U_Z with the Z-axis coordinate of the target point can be explained in terms of α_{mean}: for high Z values the angles α_{ij} decreases and the effect of the noise in the measurement results lost weight in the calculation of the Z-axis coordinate ($U_X \leq 4\ \mu m$ if $\alpha_{mean} \leq 80°$ or $Z \geq 500\ mm$ for case F).

As future work could be interesting to evaluate the effect on the measurement results when L_{ij} are dissimilar and implement the methology to the target points of a MT volumetric verification process to optimize the selection of the target points depending on the measurement uncertainty.

Acknowledgments: This research was funded by the Ministerio de Ciencia e Innovación with project number PID2022-139280OB-I00, by Aragon Government (Department of Industry and Innovation) through the Research Activity Grant for research groups recognized by the Aragon Government (T56_17R Manufacturing Engineering and Advanced Metrology Group). This is co-funded with European Union ERDF funds.

References

[1] Kunzmann H, Pfeifer T, Schmitt R, Schwenke H, Weckenmann A 2005 Productive metrology - adding value to manufacture *CIRP Ann.* **54** (2) 155-68 https:// doi.org/10.1016/S0007-8506(07)60024-9.

[2] Schwenke H, Knapp W, Haitjema H, Weckenmann A, Schmitt R, Delbressine F 2008 Geometric error measurement and compensation of machines – An update *CIRP Ann.* **57** (2) 660-75, https://doi.org/10.1016/j.cirp.2008.09.008.

[3] Ferrucci M, Haitjema H, Leach R 2018 Chapter: Dimensional Metrology in: Basics of Precision Engineering (R. Leach, S. T. Smith, R. Leach, S.T. Smith, Boca Raton), CRC Press, 151-203 978-1-4987-6085-0.

[4] De Groot P, Badami V, Liesener J 2016 Concepts and geometries for the next generation of heterodyne optical encoders *Proc. ASPE* (Portland, Oregon) **65** 146–149.

[5] Moona G,Jewariya M, Sharma R 2019 Relevance of Dimensional Metrology in Manufacturing Industries *MAPAN* **34** (1) 97–104, https://doi.org/10.1007/s12647-018-0291-3.

[6] BIPM, IEC, IFCC, ILAC, ISO, IUPAC, IUPAP, OIML 2008 International vocabulary of metrology—Basic and general concepts and associated terms, JCGM 200 Bureau International des Poids et Mesures (BIPM), 2008.

[7] Jiang X, Meng T, Wang L, Liu C 2020 Rapid calibration method for measuring linear axis optical paths of computer numerical control machine tools with a laser interferometer *Int. J. Adv. Manuf. Technol.* **110** 3347-64, https://doi.org/10.1007/s00170-020-05976-6.

[8] Zhong L, Bi Q, Wang Y 2017 Volumetric accuracy evaluation for five-axis machine tools by modeling spherical deviation based on double ball-bar kinematic test *Int. J. Mach. Tools Manuf.* **122** 106-19, https://doi.org/10.1016/j.ijmachtools.2017.06.005.

[9] Zha J,Wang T,Li L, Chen Y 2020 Volumetric error compensation of machine tool using laser tracer and machining verification *Int. J. Adv. Manuf. Technol.* **108** (7- 8) 2467-81 https://doi.org/10.1007/s00170-020-05556-8.

[10] Fan K C, Wang H, Shiou F J, Ke C W 2004 Design analysis and applications of a 3D laser ball bar for accuracy calibration of multiaxis machines *J. Manuf. Syst.* **23** (3) 194-203 https://doi.org/10.1016/S0278-6125(05)00009-9.

[11] Etalon X-AX LASERBAR, https://www.etalonproducts.com/en/products/x-ax_laserbar/, 2021 (Accessed: January 2024).

[12] Aguado S, Samper D, Santolaria J, Aguilar J J 2012 Identification strategy of error parameter in volumetric error compensation of machine tool based on laser tracker measurements *Int. J. Mach. Tools Manuf.* **53** (1) 160-9, https://doi.org/10.1016/j.ijmachtools.2011.11.004.

[13] Brosed F J, Aguilar J J, Acero R, Santolaria J, Aguado S, Pueo M 2022 Calibration and uncertainty budget analysis of a high precision telescopic instrument for simultaneous laser multilateration *Measurement* **190** 110735. https://doi.org/10.1016/j.measurement.2022.110735.

[14] BIPM, IEC, IFCC, ILAC, ISO, IUPAC, IUPAP, OIML 2008 Evaluation of Measurement Data—Guide to the Expression of Uncertainty in Measurement, JCGM 100 Bureau International des Poids et Mesures (BIPM), 2008.

[15] BIPM; IEC; IFCC; ILAC; ISO; IUPAC; IUPAP; OIML 2008 Evaluation of Measurement Data—Supplement 1 to the Guide to the Expression of Uncertainty in Measurement—Propagation of Distributions Using a Monte Carlo Method; JCGM 101 Bureau International des Poids et Mesures (BIPM), 2008.

[16] Acero R, Aguilar J J, Brosed F J, Santolaria J, Aguado S, Pueo M 2021 Design of a Multi-Point Kinematic Coupling for a High Precision Telescopic Simultaneous Measurement System *Sensors* **21** 6365 https://doi.org/10.3390/s21196365.